Chemical Geology 442 (2016) 113–120

Contents lists available at ScienceDirect

Chemical Geology

journal homepage: www.elsevier.com/locate/chemgeo

Surface reactivity of the anaerobic phototrophic Fe(II)-oxidizing bacterium *Rhodovulum iodosum*: Implications for trace metal budgets in ancient oceans and banded iron formations

Raul E. Martinez [a,*], Kurt O. Konhauser [b], Nataliya Paunova [a], Wenfang Wu [c], Daniel S. Alessi [b], Andreas Kappler [c]

[a] Institut für Geo- und Umweltnaturwissenschaften, Albert-Ludwigs-Universität, Mineralogie-Geochemie, 79104 Freiburg, Germany
[b] Department of Earth and Atmospheric Sciences, University of Alberta, Edmonton, Alberta, T6G 2E3, Canada
[c] Geomicrobiology, Center for Applied Geosciences, University of Tübingen, 72074 Tübingen, Germany

ARTICLE INFO

Article history:
Received 6 May 2016
Received in revised form 1 September 2016
Accepted 5 September 2016
Available online 12 September 2016

Keywords:
Banded iron formations
Photoferrotrophs
Cadmium sorption
Bacteria cell surface reactivity
Chemical equilibrium modeling
Anaerobic iron oxidation

ABSTRACT

It is widely accepted that anoxygenic photosynthetic bacteria (photoferrotrophs) oxidized dissolved Fe(II) in anoxic Archean seawater, leading to the sedimentation of cellular biomass and the Fe(III) minerals that comprised banded iron formations (BIF). However, it remains unknown to which extent the sedimented bacteria may have transported trace metals to BIF through their ability to sorb ions from seawater. We therefore chose the marine anoxygenic photoferrotroph *Rhodovulum iodosum* to quantify Cd^{2+}, Co^{2+}, Cu^{2+}, Mn^{2+}, Ni^{2+} and Zn^{2+} adsorption to bacteria/Fe(III)-oxyhydroxide composites at neutral pH and an ionic strength of 0.1 M. Acid base titration data were modeled using a linear programming optimization method to yield pK_a values of 4.83 ± 0.13, 6.21 ± 0.18, 7.74 ± 0.24 and 9.28 ± 0.27 and corresponding site densities of 5.7, 12.0, 3.3 and 6.5 × 10^{-4} mol/g, respectively. FTIR spectroscopy confirmed the presence of carboxyl groups as the most acidic sites corresponding to the lowest pK_a values. The analysis of Cd^{2+} sorption data showed two metal complexing sites with pK_S values of 3.44 ± 0.14 and 4.80 ± 0.21 and corresponding binding site concentrations of 1.1 ± 0.3 × 10^{-4} and 0.9 ± 0.2 × 10^{-4} mol/g on the ferrihydrite/*R. iodosum* composite. The pK_S values were used to calculate metal-ligand binding constants, K_m. This confirmed Cd^{2+} binding to the most acidic carboxyl groups on the ferrihydrite/*R. iodosum* composite surface, as the calculated K_m was consistent with reported Cd^{2+} binding constants for simple organic acids (e.g., lactic, acetic, pyruvic and citric acid). This was used to further calculate the concentration of Co^{2+}, Cu^{2+}, Mn^{2+}, Ni^{2+} and Zn^{2+} sorbed to ferrihydrite/*R. iodosum* composites. The resulting concentrations were ultimately compared to the concentrations of trace elements in BIF to demonstrate that is plausible that the trace metal content in BIF was derived from plankton growing in the ancient ocean's photic zone.

1. Introduction

Modern anoxygenic photoferrotrophs, including the marine strain *Rhodovulum iodosum*, produce biomass and Fe(III) minerals through the oxidation of Fe(II) and the use of light as the energy source (Widdel et al., 1993; Straub et al., 1999; Wu et al., 2014):

$$HCO_3^- + 4Fe^{2+} + 10H_2O \rightarrow CH_2O + 4Fe(OH)_3 + 7H^+$$

Recent studies have proposed that ancient marine photoferrotrophs utilizing a similar metabolism likely contributed to the deposition of Eoarchean (4.0–3.6 Ga) and the Paleoarchean (3.6–3.2 Ga) BIF (Craddock and Dauphas, 2011; Mloszewska et al., 2012 Czaja et al., 2013; Pecoits et al., 2015), at a time before O_2-producing cyanobacteria had evolved or produced significant amounts of O_2 (Crowe et al., 2013; Planavsky et al., 2014). Calculations using biological Fe(II) oxidation rates from freshwater and marine strains along with the chemical and physical characteristics of marine water in the Archean led to the conclusion that photoferrotrophs were capable of oxidizing the Fe(II) upwelling from deep hydrothermal sources, at rates which have been found to be in good agreement with those required to explain deposition of Fe(III) in the world's largest BIF (Konhauser et al., 2002; Kappler et al., 2005; Wu et al., 2014). Moreover, they would have had a distinct advantage over cyanobacteria because by growing deeper in the photic zone they would have had first access to the Fe(II) and nutrients being supplied by the upwelling waters (Jones et al. (2015), and recent experimental studies have demonstrated that highly ferruginous waters were toxic to cyanobacteria because high Fe^{2+} concentrations caused intracellular reactive oxygen species to accumulate within the cell leading to decreased photosynthetic efficiency and lower growth rates (Swanner et al., 2015a,b). Therefore, most current evidence points

* Corresponding author.
E-mail address: raul.martinez@minpet.uni-freiburg.de (R.E. Martinez).

http://dx.doi.org/10.1016/j.chemgeo.2016.09.004
0009-2541/

towards photoferrotrophs being the dominant marine plankton in early Archean oceans.

As a fraction of the ancient photoferrotrophic biomass settled with the iron minerals to the seafloor (Posth et al., 2010), they should have facilitated the removal of trace metals and phosphate from the water column through sorption reactions to the poorly-ordered, bacteriogenic Fe(III)-oxyhydroxides (e.g., ferrihydrite) intermixed with intact and partly degraded bacterial cells (Martinez et al., 2003; Li et al., 2011; Wu et al., 2014). One characteristic property of these aggregates is that they can strongly adsorb dissolved metal cations (Ferris et al., 1999, 2000; Lovley, 2000; Martinez et al., 2003, 2004; Borrok et al., 2004; Ueshima et al., 2008; Xiong et al., 2000; Alessi and Fein, 2010; Hohmann et al., 2011; Eickhoff et al., 2014; Robbins et al., 2013, 2015; Schmid et al., 2016). The metal binding potential of biogenic Fe(III)-oxyhydroxide/bacteria mixtures results from the type, concentration, and availability of inorganic and cell surface functional groups and their respective acidity and metal sorption constants (Kennedy et al., 2003; Martinez and Ferris, 2005).

Although a number of previous studies have examined the trace metal adsorption properties of various Fe(III)-oxyhydroxides such as ferrihydrite (Ona-Nguema et al., 2005; Xu et al., 2007; Arai, 2008; Cismasu et al., 2011; Adra et al., 2016), only a few studies have examined the reactivity of cell surfaces of photoferrotrophic cells and the resulting cell-mineral aggregates (Eickhoff et al., 2014). This is a significant shortcoming because sorption of trace metals to the same planktonic bacteria that generated the Fe(III)-oxyhydroxides in an ancient ocean may have been a means of transferring metals from the ocean's photic zone to the bottom sediment to ultimately become incorporated into BIF. Accordingly, in the present study, the Gram-negative marine photoferrotrophic strain *Rhodovulum iodosum*, originally isolated by Straub et al. (1999), was investigated for its surface proton and metal binding reactivity. Cd^{2+} was chosen as a proxy to quantify the ability of *Rhodovulum iodosum* to sorb divalent trace metal cations, as it remains soluble in seawater and the formation of Cd^{2+} carbonate or hydroxide precipitates is not significant at the experimental conditions tested here. Furthermore, Cd^{2+} provides a means to compare the metal sorption ability of *Rhodovulum iodosum* photoferrotrophs with other bacterial species, including microaerophilic Fe(II)-oxidizers (Martinez et al., 2004) and cyanobacteria (e.g., Liu et al., 2015), with different metabolisms and cell surface structures. The number of available functional groups, their acidity constants (pK_a) and concentrations, as well as the ability of *R. iodosum* to sorb Cd^{2+} were modeled using a Langmuir sorption isotherm and a linear programming optimization method (LPM). The bacterial surface was then probed with Fourier transform infrared spectroscopy (FTIR) to identify the bond types of major organic functional groups able to complex trace metals upon deprotonation at near neutral pH and high ionic strength. Finally, the complexation of other trace metal cations (e.g., Co^{2+}, Cu^{2+}, Mn^{2+}, Ni^{2+} and Zn^{2+}) were modeled to compare the quantity adsorbed to ferrihydrite/*R. iodosum* composites with those found in Earth's oldest BIF, part of the Nuvvuagittuq Supracrustal Belt in Quebec, Canada (Mloszewska et al., 2012).

2. Materials and methods

2.1. Growth of Rhodovulum iodosum bacteria

Rhodovulum iodosum was grown with Fe(II) as the electron donor under anoxic conditions. In summary, the strain *R. iodosum* was cultured using marine phototroph medium whose composition is explained in detail in Wu et al. (2014). Cultures were inoculated with Fe(II) as the electron donor and incubated at 26 °C and a constant illumination of 600 lx. *R. iodosum* was cultured with an initial Fe(II) concentration of 2 mM. Fe(II) was added from a 1 M anoxic sterile $FeCl_2$ stock solution prepared as described in Hegler et al. (2008).

2.2. Preparation of bacteria for acid/base titration and Cd sorption experiments

Aliquots of 50 mL of bacteria stock culture at the stationary growth phase were transferred to 3 sterile 50 mL Falcon® centrifuge tubes and centrifuged at 22 °C for 10 min at 13,000*g* in a high-speed centrifuge (Eppendorf® 5804). The supernatant was discarded and the centrifugation procedure was repeated twice after re-suspending the pellet in ultra-pure water (UPW) to rinse the remaining biomass. After the second rinse with UPW, the cell pellets were re-suspended in 30 mL of 0.1 M $NaNO_3$. Prior to the start of acid base titration experiments the 30 mL aliquots of background electrolyte solution containing the biomass were acidified to a pH of 3.0 with 4 μL of a 70% HNO_3 stock solution (Sigma-Aldrich® 438073 ACS reagent). A minimal loss of EPS was expected after this procedure as it follows that of Comte et al. 2006, where less than a 1% loss of EPS was observed, with most of this material being retained by the washed biomass.

For Cd^{2+} sorption experiments, aliquots were prepared as for acid base titrations; however, in this case, 100 μM Cd^{2+} were added prior to the start of the acid base titration. Cd^{2+} concentrations were measured as a function of pH (from pH 3.5 to 8.5) using a Cd^{2+} ion selective electrode (ISE) with a detection limit of 0.1 μM and prepared for measurement as described in Martinez et al. (2004). The pH range for Cd^{2+} measurements was selected to detect "free" Cd^{2+} in the absence of carbonate, hydroxide or chloride complexes. The Cd^{2+} ISE was calibrated prior to each experimental run and a Nernstian response with a 28.7 ± 0.4 mV slope was obtained.

Acid base titration and metal sorption experiments were carried out in a 0.1 M $NaNO_3$ background electrolyte concentration to avoid cation interference with Cd^{2+} ion selective and pH electrode measurements. According to the work of Martinez et al. (2002), acid dissociation constants and binding site concentrations under this conditions can be extrapolated to higher ionic strengths (e.g. IS = 0.5 M) as no significant electrostatic effects on these parameters were observed in the presence of Gram-negative or Gram-positive bacteria species.

2.3. Titration of biomass and automatic titrator settings

Acidified bacteria aliquots, prepared for acid base or Cd^{2+} adsorption experiments as described previously, were transferred to a glass titration vessel (Metrohm® 6.1415.310) covered with an air tight lid (Metrohm® 6.1414.010) through which a pH electrode and a custom-designed N_2 gas line interface were fitted. The pH electrode (Metrohm® 6.0257.000) was connected to an autotitrator system (Metrohm® Titrino 719S) interfaced with Metrohm® Tinet 2.5 software to a personal computer. It was four point calibrated with NIST standard buffers (i.e. 4.01, 6.86, 9.01, 11.01) before each experiment. The slope in all cases was >95% of the Nernstian value. The system was equilibrated for a period of 30 min before the start of the acid base titrations. The drift criterion for the pH electrode was set to 0.1 mV/min. The titrations were conducted in the pH range of 3.0 to 11.0. Vacuum filtration was used to determine the dry weight of bacteria as described earlier in Martinez et al. (2002). The raw acid-base titration data was transformed for the determination of bacteria surface functional group concentrations and acidity constant values (pK_a) as summarized below and as explained in Martinez et al. (2002).

2.4. Modeling of acid base titration data

Bacteria cell surface groups, denoted by L_j^-, deprotonate as a function of increasing pH:

$$HL_j \overset{K_{a(j)}}{\rightarrow} H^+ + L_j^- \quad (1)$$

where j = 1 to n functional groups, HL_j and L_j^- correspond to the concentration of protonated and deprotonated groups respectively, and $K_{a(j)}$ is the acidity constant for group j such that pK_a ($-\log_{10} K_a$). In this study, acid base titration data was transformed and analyzed as explained in Martinez et al. (2002) to determine the number and concentration, $[L_j^-]$, of bacteria surface deprotonated functional groups. $[L_j^-]_{exp}$, was derived from experiment as:

$$\left[L_j^-\right]_{exp} = Cb_i + Ca_i + \left[H^+\right] - [OH^-] \tag{2}$$

where i = 1 to m titrant additions (i.e. 0.1 M NaOH), Ca_i and Cb_i represent the acid and base concentrations, respectively, at the ith addition of titrant and $[H^+]$ and $[OH^-]$ are obtained from measured pH. As described by Martinez et al. (2002), the concentration of deprotonated groups in Eq. (2) can be determined from measured ($[H^+]$) and adjustable ($K_{a(j)}$ and $[L_j^-]$) parameters. From the total surface functional group, ($L_{T(j)}$), mass balance:

$$L_{T(j)} = \left[HL_j\right] + \left[L_j^-\right] \tag{3}$$

and the expression for the acid dissociation constant, K_a, in Eq. (1),

$$K_{a(j)} = \frac{\left[H^+\right]\left[L_j^-\right]}{\left[HL_j\right]} \tag{4}$$

A calculated concentration of deprotonated cell surface functional groups, $[L_j^-]_{calc}$, can be derived for m titrant additions and n surface functional groups, as explained in detail in Martinez et al. (2002):

$$\left[L_j^-\right]_{calc} = \alpha_{ij} \times L_{T(j)} = \sum\nolimits_{j=1}^{\lambda} \left(\frac{K_{a(j)}}{K_{a(j)} + \left[H^+\right]}\right) \times L_{T(j)} \tag{5}$$

where, α_{ij} refers to the fraction of deprotonated ligand j giving rise to the concentration of deprotonated surface groups, $[L_j^-]_{calc}$. Linear programming optimization (LPM) for determination of acidity constants, described in detail in Brassard et al. (1990) and Cox et al. (1999), was used to calculate $[L_j^-]_{calc}$ by minimizing the error difference between Eqs. (2) and (5). This method used a 0.2 fixed interval pK_a grid ranging from 3 to 11 to which best-fit values of $L_{T(j)}$ were assigned (Brassard et al., 1990; Cox et al., 1999; Martinez et al., 2002).

2.5. Modeling of Cd^{2+} sorption to R. iodosum

Data from experiments involving Cd^{2+} complexation to *Rhodovulum iodosum* photoferrotrophic bacteria-iron oxide composites were modeled using a Langmuir isotherm approach along with linear programming (LPM) optimization, as described previously in detail by Martinez et al. (2004). A competition reaction of between Cd^{2+} and H^+ was assumed for deprotonated groups (L_j^-) on the bacteria reactive surface:

$$L_jH^0 \overset{K_{a,j}}{\leftrightarrow} H^+ + L_j^- \tag{6}$$

$$Cd^{2+} + L_j^- \overset{K_{m,j}}{\leftrightarrow} CdL_j^+ \tag{7}$$

$$\text{Overall mechanism}: Cd^{2+} + L_jH^0 \overset{K_{S,j}}{\leftrightarrow} CdL_j^+ + H^+ \tag{8}$$

where, $K_{a,j}$ is the acid dissociation constant (Eq. 4), $K_{m,j}$ is the metal-surface ligand association constant and $K_{S,j}$ is the ionic strength dependent apparent metal-bacteria/Fe(III)-oxyhydroxide composite adsorption equilibrium constant for the reaction in Eq. (8), such that $K_{S,j} = K_{a,j} * K_{m,j}$ and can be defined as:

$$K_{S,j} = \frac{\left[CdL_j^+\right]_i \cdot \left[H^+\right]_{meas,i}}{\left[Cd^{2+}\right]_{meas,i} \cdot \left[L_jH^0\right]_i} \tag{9}$$

for i = 1…n titrant additions and j = 1…m binding sites. $K_{S,j}$ is a function of proton and metal concentrations, ($[H^+]_{meas,i}$and $[Cd^{2+}]_{meas,i}$) and of the amount of Cd^{2+} bound to the jth site at the ith step of the titration, $[CdL_j^+]_i$. The total bound metal at the ith titrant addition determined from experiment, $[CdL^+]_{T,i}$, can be expressed as:

$$\left[CdL^+\right]_{T,i} = \sum_{j=1}^{m}\left[CdL_j^+\right]_i = \left[Cd^{2+}\right]_T - \left[Cd^{2+}\right]_{meas,i} \tag{10}$$

and

$$[L]_T = \sum_{j=1}^{m}[L_j] = \left[CdL^+\right]_{T,i} + \sum_{j=1}^{m}\left[L_jH^0\right]_i \tag{11}$$

where $[L]_T$ is the total ligand mass balance and $[L_j]$ refers to the concentration of the bacteria surface jth functional group. The total concentration of bound metal, $[CdL^+]_{T,i}$, can then be expressed as a sum of complexed metal concentrations for each of the jth surface ligands at the ith step of the titration ($[CdL^+]_{T,i} = \sum_{j=1}^{m}[CdL_j^+]_i$). From the total ligand mass balance and the expression for the metal adsorption constant in Eq. (9), an objective function designed for linear programming optimization can be obtained by expressing the total calculated bound metal concentration at the ith titrant addition,$[CdL^+]_{T,calc,i}$, as a function of measured, ($[H^+]_{meas,i}$ and $[Cd^{2+}]_{meas,i}$) and adjustable ($[L_j]$) parameters, as shown below:

$$\begin{aligned}\left[CdL^+\right]_{T,calc,i} &= \sum_{j=1}^{m}\left(\alpha_{ML,ij} \cdot \left[L_j\right]\right) \\ &= \sum_{j=1}^{m}\left(\frac{\left[Cd^{2+}\right]_{meas,i} \cdot K_{S,j}}{\left[Cd^{2+}\right]_{meas,i} \cdot K_{S,j} + \left[H^+\right]_{meas,i}} \cdot \left[L_j\right]\right)\end{aligned} \tag{13}$$

As described in detail in Martinez and Ferris (2001), Martinez et al., 2004), the LPM approach assigns values of $[L_j]$ to a corresponding $K_{S,j}$ on a fixed interval pK_S grid by minimizing the absolute error, $e = [CdL^+]_{T,calc,i} - [CdL^+]_{T,i}$. This method finds one global minimum for the error function, avoiding convergence problems (Brassard et al., 1990; Smith and Kramer, 1999; Martinez and Ferris, 2001; Martinez et al., 2004).

2.6. XRD, SEM imaging and FTIR measurements of ferrihydrite/R. iodosum composites

The mineralogical analysis of the ferrihydrite/*Rhodovulum iodosum* composites was done by powder X-ray diffraction (XRD) at the University of Freiburg. The XRD spectra were collected at a step size of 0.02° and a dwell time of 1 s per step from a 2θ of 4° to 80°. The XRD patterns were evaluated with the DIFFRACplus 5.0 software. Scanning electron microscopy (SEM) of ferrihydrite/*R. iodosum* composites was performed in the Center for Applied Geoscience at the University of Tübingen, as described previously by Wu et al. (2014). For SEM sample preparation, ~1 mL of culture was taken, washed with Millipore water, and centrifuged. The pellet was re-suspended in acetone, and one drop was placed onto a sticky carbon pad mounted on an aluminum stub (both Plano GmbH, Wetzlar, Germany), and dried in a vacuum chamber (0.9 bar). The sample was sputter-coated with 6–8 nm platinum (BAL-TEC SCD 005, BAL-TEC, Liechtenstein, 35 mm working distance, 30 mA, 60 s).

Fourier transform infrared (FTIR) spectroscopy measurements were performed in the Organic Chemistry Department at the University of Freiburg with a Perkin Elmer® FTIR Spectrometer. FTIR spectra were collected at a 2 cm^{-1} resolution and 256 interferograms. Spectra were recorded for both background and sample material within an optical range from 4000 to 400 cm^{-1}. For FTIR measurements, 2 mg of the ferrihydrite/*R. iodosum* composites were freeze-dried and homogeneously mixed with 250 mg of dry potassium bromide (KBr – 99.9% Sigma-Aldrich) to prepare a KBr pellet for FTIR measurements.

3. Results and discussion

3.1. Composition of the ferrihydrite/R. iodosum composites

XRD analysis of ferrihydrite/*Rhodovulum iodosum* composites showed two broad peaks at 2θ values of 65.3° and 33.7° (data not shown). This result suggests the presence of 2-line ferrihydrite, a poorly ordered fine-grained Fe(III) oxyhydroxide which precipitates as a consequence of the biological oxidation of Fe(II) (Swanner et al., 2015a,b).

SEM imaging (Fig. 1) of *Rhodovulum iodosum* bacteria revealed that cells were associated with, but not encrusted with, biogenic ferrihydrite. As described in previous studies, cell encrustation is impeded by exopolymeric substances (EPS) that serve as nucleation sites for mineral phases, including Fe(III)-oxyhydroxides (Konhauser, 1997, 1998; Schaedler et al., 2009; Schmid et al., 2016; Franzblau et al., 2014, 2016). We observed in *R. iodosum* samples (Fig. 1) that the mineral phase was associated with an organic fiber network structure, usually characteristic of biofilm EPS. In order to account for the functional groups present in the ferrihydrite/*R. iodosum* composites, FTIR analyses were performed (Table 1). In the absence of Cd^{2+}, FTIR spectroscopy showed weak absorption bands from 900 to 800 cm^{-1}. These were attributed to a polysaccharide signature consistent with the lipopolysaccharide (LPS) chain structure of a Gram-negative bacterial surface. Absorption bands characteristic of ferrihydrite, such as —O—H and Fe—O stretches at 322 and 935 cm^{-1}, respectively, were not observed. Similar stretching modes for goethite at 766 and 957 cm^{-1} were absent. These results suggest a greater absorption of infrared radiation by organic matter bond types, whose peak intensities may overlap with those of the ferrihydrite fraction.

Table 1 shows a detailed summary of the FTIR absorption bands from spectra recorded in the presence of ferrihydrite/*R. iodosum* composites. The absorption band at 3262 cm^{-1} may be indicative of the presence of trace water in the sample. However, LPS also contains terminal carboxylic groups bound to α-Kdo-(2→8)-α-kdo allyl disaccharide subunits (kdo = 3-Deoxy-D-*manno*-oct-2-ulosonic acid) (Omoike and Chorover, 2004; Parikh and Chorover, 2007), suggesting that the band observed at >3000 cm^{-1} would be the result of a —O—H stretch for carboxylic acids expected in the range of 3300 to 2500 cm^{-1} (Tamm and Tatulian, 1997; Jiang et al., 2004). The presence of this —OH group is further supported by absorption bands at 1441 and 913 cm^{-1} assigned to the —OH bend of carboxylic acids reported previously at 1440–1395 and 950–913 cm^{-1} (Tamm and Tatulian, 1997; Barth, 2000). A further absorption at 1806 cm^{-1} can be assigned to a shift of the carboxylic —C═O stretch expected in the range of 1760 to 1690 cm^{-1} (Tamm and Tatulian, 1997; Omoike and Chorover, 2004). For example, side chains of the amino acids, Glu and Asp, have shown a characteristic absorption from their —COO^- moieties extending from 1404 to 1402 cm^{-1} (Barth, 2000). These values are consistent with that in Table 1 at 1401 cm^{-1}, suggesting the existence of —COO^- groups in the ferrihydrite/*R. iodosum* composite surface (Omoike and Chorover, 2004).

Table 1 also shows absorption bands at 1015, 913, 804 and 798 cm^{-1}. These fall within the range of the polysaccharide fingerprint region (Parikh and Chorover, 2007), and do not correspond to characteristic ferrihydrite absorptions. For organic components containing phosphate or hydrogen phosphate, absorption bands were observed at 1020 cm^{-1}, for example, for dioctadecylhydrogen phosphate (Abramson et al., 1965; Omoike and Chorover, 2004). This is consistent with the value of 1022 cm^{-1} in Table 1, suggesting the additional presence of hydrogen phosphate on the surface of the ferrihydrite/*R. iodosum* composites. Characteristic amide II absorptions range between 1650 and 1620 cm^{-1} (Tamm and Tatulian, 1997; Barth, 2000). These values correspond with that of 1641 cm^{-1} in Table 1, which would indicate the presence of —C—N stretching and —N—H bending vibrational models on the ferrihydrite/*R. iodosum* composite surface. Further absorption bands at 744 and 1296 cm^{-1} (Table 1) suggest the presence of —CH_2 rocking and wagging band progression from bacteria cell membrane lipids (Tamm and Tatulian, 1997; Jiang et al., 2004).

Table 1
Main FTIR absorption bands from the *Rhodovulum iodosum*/iron(III) (oxyhydr)oxide composite (Tamm and Tatulian, 1997; Jiang et al. 2004).

Frequency (cm^{-1})	Assignment
3262	—O—H stretching (carboxylic acid group)
1806	—C═O stretching (from carboxylic acid group)
1641	Amide II absorption band (—C—N stretching and —N—H bending)
1441	—O—H bend absorption in carboxylic acid group
1401	Symmetric stretching of carboxylate anion (−COO^-)
1296	—C—O stretching (carboxylic acid group)
1022	—P—OH stretching (phosphate/hydrogen phosphate groups)
1015	Polysaccharide absorption band (fingerprint region)
913	—O—H bend in carboxylic acid, absorption in the polysaccharide finger print region.
804	Polysaccharide absorption band (fingerprint region), and indication of —P—O antisymmetric stretch.
798	Polysaccharide absorption band (fingerprint region)

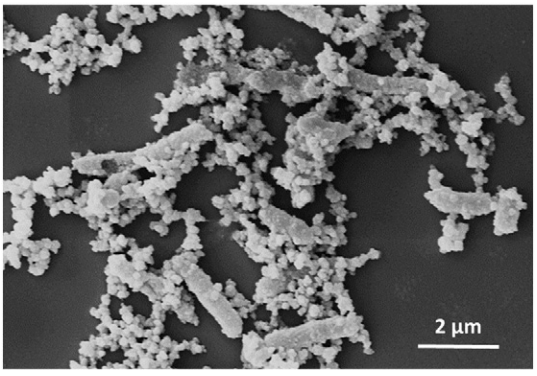

Fig. 1. Scanning electron micrograph of *Rhodovulum iodosum* ferrihydrite composites. Fe(III)-oxyhydroxides are observed to be partially associated with bacterial cells and on filamentous EPS-like structures.

3.2. Reactivity of ferrihydrite/R. iodosum composites

Table 2 presents a summary of the results obtained from the modeling of acid base titration data with linear programming optimization to generate a best fit of the experimental charge excess (Eq. 2) by the objective function in Eq. (5). This approach yielded reactive solid surface binding site concentrations of 5.7 ± 0.2, 10.0 ± 0.4, 7.3 ± 0.3 and 5.5 ± 0.6 × 10^{-4} mol/g of ferrihydrite/*R. iodosum* composite with corresponding pK_a values of 4.85 ± 0.05, 6.15 ± 0.05, 7.75 ± 0.05 and 9.20 ± 0.05. SEM, XRD and FTIR analyses confirmed the presence of intact *R. iodosum* cells, ferrihydrite, and a bacterial-derived organic fiber network. The nature of this structure, for the same bacteria species under the equal growth conditions, was investigated previously by Wu et al. (2014), and determined to consist of EPS. The pK_a values in Table 1 are consistent with those recorded for Gram-negative bacteria in the absence of iron (oxyhydr)oxides (Martinez et al., 2002). This strongly suggests that these values, obtained from LPM analyses of acid base

Table 2
Results from linear programming optimization of acid base titration data for *R. iodosum*/bacteriogenic iron oxyhydroxide composite.

Surface site	Mean pK_a[a]	Site concentration (10^{-4} mol/g bacteria)[**]	Suggested functional group
1	4.85 ± 0.05	5.7 ± 0.2	Carboxyl
2	6.15 ± 0.05	10.0 ± 0.4	Carboxyl or phosphoryl
3	7.75 ± 0.05	7.3 ± 0.6	Amine
4	9.20 ± 0.05	5.5 ± 0.3	Amine

[a] pK_a where assigned best fit site concentrations as per the fitting of experimental data by the model in Eq. (5).
[**] Optimal value of site concentration as determined by the model in Eq. 5.

titration data, were generated by reactive surface functional groups on intact *R. iodosum* cells and the corresponding associated organic matter (i.e., EPS). The obtained acidity constants are further consistent with the results of previous studies dealing with the quantification of bacteriogenic iron oxides, where the surface reactivity of such mixtures was dominated by contributions from reactive groups associated with the bacteria cell fraction, with pK_a values coinciding with those in this study (Martinez et al. 2003; Mikutta et al. 2012; Moon and Peacock, 2013).

The pK_a of 4.85 ± 0.05 in Table 1 is in good agreement with the value of 4.80 ± 0.54 reported previously for the bacterial fraction of a ferrihydrite-cell composite, generated in the presence of a microaerophilic, Fe(II)-oxidizing species (e.g., *Gallionella ferruginea*) (Martinez et al., 2003). This value is also consistent with a pK_a of 4.85 ± 0.71 resulting from modeling the surface acid base properties of the Gram-negative bacterium, *Escherichia coli* (Martinez et al., 2002). This acidic pK_a was attributed to the presence of carboxyl functional groups on the ferrihydrite/*R. iodosum* composite surface, in agreement with previous studies (Fein et al., 1997). The acidity constant at 6.15 ± 0.05 was assigned to the presence of phosphoryl and carboxyl groups, as suggested by FTIR analysis, and it is consistent with previously determined acidity constant values for Gram-negative bacteria (Fein et al., 1997; Cox et al., 1999; Phoenix et al., 2002; Martinez et al., 2002).

Analysis of acid base titration data from the ferrihydrite/*R. iodosum* composite revealed the presence of two further binding sites on the reactive solid surface, with pK_a values of 7.75 ± 0.05 and 9.20 ± 0.05. The latter indicates the presence of amine groups associated with the cell surface, as suggested by FTIR measurements herein. The pK_a value of 7.75 ± 0.05 (Table 2) is in good agreement with acidity constants in the range of 7.47 ± 0.52 and 7.89 ± 0.88 reported for Gram-negative bacteria and bacteriogenic Fe(III) oxyhydroxides respectively (Martinez et al., 2002, 2003). The binding site concentrations in Table 2 show that the surface charge excess is mostly dominated by acidic deprotonated organic groups (i.e. $>COO^-$ and $>PO_4^{2-}$).

3.3. Cadmium adsorption to biomass-mineral composites

The presence of organic surface functional groups, as suggested by FTIR spectroscopy and as detected through acid base titration modeling, indicate the ability of the ferrihydrite/*R. iodosum* composite surface to adsorb metal cations at near neutral pH and high ionic strength. Chemical equilibrium speciation calculations done prior to the Cd^{2+} sorption experiments for a solution containing 100 μM Cd^{2+} in a 0.1 M $NaNO_3$ electrolyte showed a significant presence of cadmium hydroxide aqueous species (i.e., $Cd(OH)^+$ and $Cd(OH)_2^0$) only at a pH >8.5. Under similar conditions the dissolution of Fe(III)-oxyhydroxides generated by *R. iodosum* only becomes important at pH values lower than 3.5 (Martinez et al., 2003, 2004). For these reasons, experiments were designed to address the sorption of "free" Cd^{2+} and preserve the surface reactive properties of ferrihydrite/*R. iodosum* composites within the pH range of 3.5 to 8.5. The metal binding experiments reported herein, therefore, extended from overall pH ranges of 4.02 ± 0.09 to 8.24 ± 0.04, respectively, and acid base titrations from an average pH of 3.46 ± 0.11 to 10.24 ± 0.19.

Cd^{2+} complexation to the ferrihydrite/*R. iodosum* composite was assessed using linear programming optimization model for metal sorption as described previously (Martinez and Ferris, 2001; Martinez et al., 2004). The Cd^{2+} sorption constants, obtained by fitting experimental metal sorption data with the Langmuir isotherm approach as per Eq. (13), are conditional upon ionic strength, and implicitly embody electrostatic parameters as previously described (Brassard et al., 1990; Cox et al., 1999; Smith and Ferris, 2001; Martinez et al., 2002, 2004). Fig. 2 shows four replicate Cd^{2+} sorption experiments. The solid line indicates the best fit of the metal sorption data onto the ferrihydrite/*R. iodosum* composite. The fitting of the objective function in Eq. (13) to experimental data resulted in two metal binding sites with sorption constants (pK_S) of 3.44 ± 0.14 and 4.80 ± 0.21, and corresponding site concentrations of 1.1 ± 0.3 × 10^{-4} and 0.9 ± 0.2 × 10^{-4} mol/g of reactive solid. A decrease in the pK_S values (i.e. from 4.80 ± 0.21 to 3.44 ± 0.14) indicates a stronger binding of Cd^{2+} to the solid surface. This is consistent with the higher binding site concentration of 1.1 ± 0.3 × 10^{-4} mol/g.

Although the precise nature of these sites cannot be accurately determined from surface complexation modeling, the results herein are in good agreement with previous studies for the Gram negative *Escherichia coli* (Gram-negative species) where two Cd^{2+} binding sites were observed (Martinez and Ferris, 2001). The feasibility of using the LPM approach, to investigate trace metal adsorption on bacteria cell surfaces, can be supported by the results from spectroscopy measurements. For example, Boyanov et al. (2003) determined three Cd^{2+} complexing functional groups on the *Bacillus subtilis* surface (including $>COO^-$, $>PO_4^{2-}$) based on the interpretation of EXAFS spectra. This result is in good agreement with our results of FTIR spectroscopy and the two metal binding sites found by LPM optimization of metal adsorption data from the ferrihydrite/*R. iodosum* composite surface.

As shown in Table 2, the two most acidic sites on the ferrihydrite/*R. iodosum* composite were assigned to carboxyl functional surface groups. As mentioned previously, a lower value of pK_S indicates a tighter

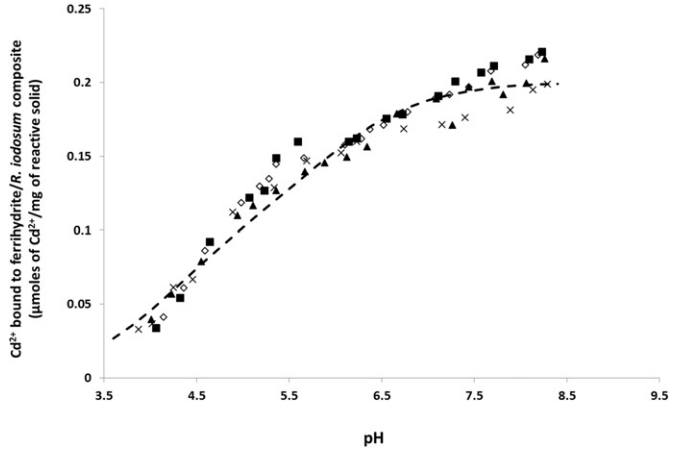

Fig. 2. Cd^{2+} sorption replicate sorption experiments performed for 100 μM Cd^{2+} in the presence of *Rhodovulum iodosum* ferrihydrite composites. Squares, triangles, circles and cross markers correspond to replicate experiments for a solution of 0.1 M $NaNO_3$ as described in text. The dotted line corresponds to the fit of experimental data from the optimization of experimental data (Eq. 10) with the objective function described by Eq. (13).

binding of Cd^{2+} to the reactive solid surface. The pK_S of 3.44 ± 0.14 suggests interaction of Cd^{2+} with the most acidic (deprotonated) organic sites with a pK_a of 4.85 ± 0.05. Similarly, the weaker Cd^{2+} sorption shown by the pK_S of 4.80 ± 0.21 corresponds to the less acidic pK_a value of 6.15 ± 0.05. Calculation of the metal-ligand association constant, $K_{m,j}$, for Cd^{2+} to >COO^- groups on the ferrihydrite/*R. iodosum* composite yielded $\log_{10} K_{m,j}$ values of 1.41 ± 0.15 and 1.35 ± 0.22. These values were compared to metal association constants describing Cd^{2+} binding to simple deprotonated carboxylic acids at near neutral pH and an ionic strength of 0.1 M (Martell and Robert, 1999). Cd^{2+} binding to mono-protic acid sodium salts, such as pyruvate, lactate and acetate show $\log_{10} K_{m,j}$ values of 0.69, 1.30 and 1.56 respectively (Martell and Robert, 1999). Literature results indicated a $\log_{10} K_{m,j}$ of 1.30 for Cd^{2+} binding with the most acidic deprotonated >COO^- group of citric acid at near neutral pH (Martell and Robert, 1999). The agreement between the experimental and reported $\log_{10} K_{m,j}$ values emphasizes the validity of the modeling approaches in this study, showing their ability to quantify acidity and metal sorption constants on the surface of complex reactive solids. Based on the experimental data in Fig. 2, the amount of Cd^{2+} bound to the ferrihydrite/*R. iodosum* composite at near-neutral pH and an ionic strength of 0.1 M was 0.21 ± 0.01 μmol of metal/mg of reactive solid.

The values of $\log_{10} K_{m,j}$ for Cd^{2+} binding to carboxylic acid groups on the ferrihydrite/*R. iodosum* composite are consistent with those reported in the literature for Cd^{2+} interaction with simple deprotonated organic acids at near-neutral pH and an ionic strength of 0.1 M (Martell and Robert, 1999). Accordingly, the complexation of metal cations, such as Co^{2+}, Cu^{2+}, Mn^{2+}, Ni^{2+}, and Zn^{2+}, to the most acidic sites of the ferrihydrite/*R. iodosum* composite can then be quantified. For a monodentate metal cation/carboxylate interaction, average $\log_{10} K_{m,j}$ of 1.04 ± 0.31, 2.18 ± 0.27, 1.24 ± 0.30, 1.34 ± 0.14 and 1.35 ± 0.31 were taken from literature for Co^{2+}, Cu^{2+}, Mn^{2+}, Ni^{2+} and Zn^{2+}, respectively. These values were obtained from the interaction of the metals with organic carboxylate groups, namely pyruvate, lactate and acetate, and citrate (Martell and Robert, 1999). These $\log_{10} K_{m,j}$ were used to calculate the amount of Co^{2+}, Cu^{2+}, Mn^{2+}, Ni^{2+}, or Zn^{2+} bound to the ferrihydrite/*R. iodosum* composite. From the concentration of deprotonated carboxyl groups (calculated as a function of pH), and the fraction of metal bound to the deprotonated ligands ($\alpha_{CdL} = K_{m,j} * [L^-] / (K_{m,j} * [L^-] + 1)$, concentrations of 0.10 ± 0.01, 1.24 ± 0.02, 0.20 ± 0.01, 0.16 ± 0.01, and 0.21 ± 0.01 μmol of metal/mg of reactive solid for [CoL^+], [CuL^+], [MnL^+], [NiL^+], and [ZnL^+], respectively, within the pH range of 6.8 to 7.2.

3.4. Other trace metals and importance for BIF

If cell biomass-ferrihydrite aggregates formed in the water column of an Eoarchean ocean, the question is whether they were a major contributor to the trace element inventory of BIF deposited at that time, as illustrated by the schematic in Fig. 3. To address this question, we first calculated the amount of ferric iron deposited in an annual BIF layer. It has been estimated that during periods of rapid ferric hydroxide deposition generated through the activity of photoferrotrophs, 1 mm/year of unconsolidated sediment was deposited (Konhauser et al., 2005). In addition, based on an initial deposit of 80% $Fe(OH)_3$ and 20% amorphous SiO_2 (consistent with the 80% hematite/magnetite and 20% quartz now displayed as Fe-rich mesobands in oxide-type BIF; Konhauser et al., 2005), with corresponding densities of 3.8 g cm^{-3} and 2.2 g cm^{-3}, respectively, and a Fe_{Total} of 42%, the annual quantity of Fe deposited could have been in the order of 26.05 mol m^{-2}. Based on reported Fe(II) oxidation rates for *Rhodovulum iodosum* of 0.15 mM Fe(II) day^{-1} at 4.07 mM Fe(II) at 12 μmol quanta m^{-2} s^{-1} light intensity and a cell density of 2.3×10^8 cells ml^{-1}, Wu et al. (2014) calculated that each individual cell can oxidize 4.11×10^{-12} mol Fe(II) $year^{-1}$. At a calculated annual precipitation rate of 26.05 mol m^{-2}, approximately 6.34×10^{12} metabolizing cells of *R. iodosum* would have been needed to account for the ferric iron sedimentation rate. Assuming a 100-m-deep photic zone, then a minimum cell density of 6.34×10^4 cells ml^{-1} were required to precipitate an annual BIF layer.

Table 3 presents the average trace metal composition in magnetite from Earth's oldest BIF, the Nuvvuagittuq Supracrustal Belt in Quebec, Canada (see Mloszewska et al., 2012 - their Table 1), and how much metal is estimated to have been sedimented annually during BIF deposition. As an example, the concentration of Mn in an Fe-rich mesoband had a mean value of 156.0 mg/kg, resulting in a maximum annual deposition of 1.09×10^{-2} mol for each m^2 of BIF sediment. Based on an average cell volume of 1.5 μm^3 for *R. iodosum* (Straub et al., 1999), a proportionate mass to *Gallionella* (where each cell has a volume of 1 μm^3 and a wet mass of 1.3×10^{-12} g; Hallbeck and Pedersen, 1991), and the surface complexation model in our study, we can further calculate the amount of those same metals adsorbed to the 6.34×10^{12} metabolizing cells calculated above. From Table 3 it is apparent that adsorption to biomass with a population of cells on the order of 6.34×10^4 cells ml^{-1} can account for all the Co (1.3×), Cu (120×) and Cd (3.72×) annually incorporated into a BIF layer. Insufficient amounts of Mn (0.17×), Ni (0.25×) and Zn (0.53×) were provided by the biomass.

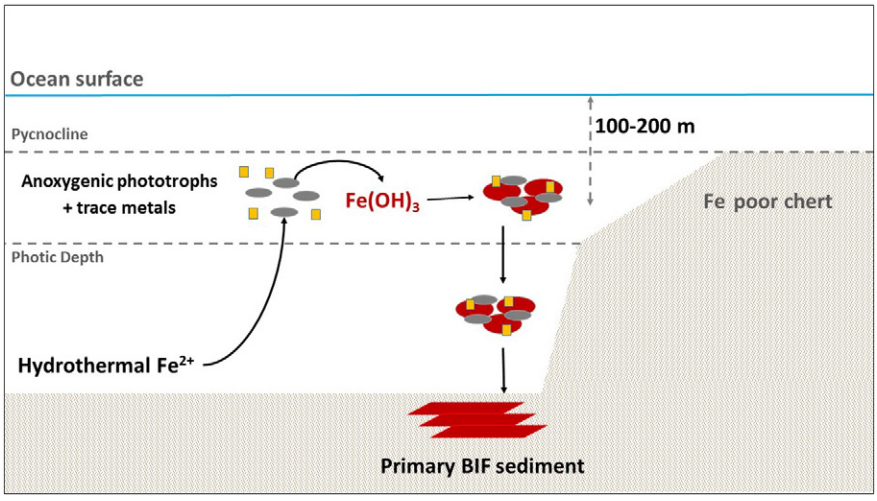

Fig. 3. Schematic figure showing an ancient ocean environment with anoxygenic phototrophic Fe(II) oxidation, indicating trace metal adsorption to formed cell-mineral aggregates, which then sediment to the ocean floor and are later incorporated in BIFs.

Table 3
Trace metal composition in the Nuvvuagittuq banded iron formation and potentially adsorbed by a community of *Rhodovulum iodosum* cells.

	Mn	Co	Ni	Cu	Zn	Cd
Fe-rich mesoband composition						
Average concentration (mg/kg)*	156.00	11.27	93.61	1.62	63.63	1.57
Mesoband mass/year (kg)	3.84	3.84	3.84	3.84	3.84	3.84
Amount in annual BIF layer (mg)	599.04	43.28	359.46	6.22	244.34	6.03
Molecular mass (mg/mol)	54,938	58,933	58,693	63,546	65,380	11,241
Amount in annual BIF layer (moles)	1.09E−02	7.34E−04	6.12E−03	9.79E−05	3.74E−03	5.36E−04
Rhodovulum - adsorption						
Cell mass (mg)**	1.50E−09	1.50E−09	1.50E−09	1.50E−09	1.50E−09	1.50E−09
Number of cells needed to form 1 m^2 of BIF	6.34E+12	6.34E+12	6.34E+12	6.34E+12	6.34E+12	6.34E+12
Total biomass (mg)	9.51E+03	9.51E+03	9.51E+03	9.51E+03	9.51E+03	9.51E+03
Metal adsorbed via SCM (μM/mg biomass)	0.20	0.10	0.16	1.24	0.21	0.21
Total amount of metals adsorbed (moles)	1.90E−03	9.51E−04	1.52E−03	1.18E−02	2.00E−03	2.00E−03
Adsorption excess	0.17	1.30	0.25	120.46	0.53	3.72

Note: average concentration in BIF from Mloszewska et al. (2012)* and proportionate cell mass from Hallbeck and Pedersen (1991)**.

The values given in Table 3 should be viewed with some caution as we did not take into account competitive adsorption, i.e., the amount of each metal adsorbed when all are available in solution. We also did not consider that only some planktonic photoferrotrophs would have been sedimented along with the ferrihydrite because a fraction of cells are capable of remaining unattached from the iron minerals (e.g., Posth et al., 2010; Gauger et al., 2016). Similarly, some biomass will be recycled within the water column before reaching the seafloor (e.g., Konhauser et al., 2005). Nonetheless, the calculations do drive home the message that the chemical reactivity of bacterial plankton can remove a significant amount of trace metals from seawater. Moreover, we have only considered the reactivity of *R. iodosum*, and not the sum reactivity of all plankton living in the photic zone, including other phototrophs and chemoheterotrophs. For instance, using modern seawater cell densities on the order of 10^6 cells ml^{-1} (Azam et al., 1983), which translates into a total biomass of 10^{14} cells or 1.5×10^5 mg of biomass, and assuming that all of those cells are similarly reactive, then the magnitude of metals adsorbed increases significantly over the same 100 m deep water column. In fact, every metal in BIF can be accounted for: Mn (2.75×), Co (20.43×), Ni (3.92×), Cu (1900.01×), Zn (8.43×) and Cd (58.73×). Similarly, if we were to consider a water column depth of 200 m –the depth of the modern continental shelf (Menard and Dietz, 1951) – and a cell density of 10^6 cells ml^{-1}, then the amount of metal adsorbed and sedimented doubles.

4. Conclusion

This study quantified the ability of *Rhodovulum iodosum* to bind Cd^{2+} at near neutral pH conditions and high ionic strength. This study further demonstrates that organic functional groups are the dominant fraction of the reactive solid surface composite of bacteria and Fe(III)-oxyhydroxide. Two Cd^{2+} binding sites were obtained from surface complexation modeling and linear programming optimization. The sorption and acidity constants optimized from acid base titration and metal sorption experiments indicate a strong binding of Cd^{2+} to the most acidic organic functional groups (e.g. $>COO^-$) on the bacteria surface. From FTIR analyses, this Cd^{2+} adsorption corresponds to a combination of carboxyl and phosphoryl containing organic structures on the cell surface. The ability of *Rhodovulum iodosum* species to complex trace elements is an important step forward in determining the biogenic origin of trace metals in ancient sediments, such as BIF.

Acknowledgements

REM would like to thank the Institute of Geoscience and the Faculty of Earth and Environmental Science at the University of Freiburg (Science Support Center (SSC) Innovations fonds Forschungs Kapitel: 1410, TG 99, BA 600197) for providing the funding for this research project. KOK and DSA would like to thank the Natural Sciences and Engineering Research Council of Canada (NSERC). The authors would also like to thank Dr. Jan. Dirksen of the Organic Chemistry Department at the University of Freiburg for his assistance with FTIR measurements.

References

Abramson, M.B., Norton, W.T., Katzman, R., 1965. Study of ionic structures in phospholipids by infrared spectra. J. Biol. Chem. 240, 2389–2395.
Adra, A., Morin, G., Ona-Nguema, G., Brest, J., 2016. Arsenate and arsenite adsorption onto Al-containing ferrihydrites. Implications for arsenic immobilization after neutralization of acid mine drainage. Appl. Geochem. 64, 2–9.
Alessi, D.S., Fein, J.B., 2010. Cadmium adsorption onto mixtures of soil components: testing the component additivity approach. Chem. Geol. 270, 186–195.
Arai, Y., 2008. Spectroscopic evidence for Ni(II) surface speciation at the iron oxyhydroxides-water interface. Environ. Sci. Technol. 42, 1151–1156.
Azam, F., Fenchel, T., Field, J.G., Gray, J.S., Meyer-Reil, L.A., Thingstad, F., 1983. The ecological role of water-column microbes in the sea. Mar. Ecol. Prog. Ser. 10, 257–263.
Barth, A., 2000. The infrared absorption of amino acid side chains. Prog. Biophys. Mol. Biol. 74, 141–173.
Borrok, D., Fein, J.B., Kulpa, C.F., 2004. Proton and Cd adsorption onto natural bacterial consortia: testing universal adsorption behavior. Geochim. Cosmochim. Acta 68, 3231–3238.
Boyanov, M.I., Kelly, S.D., Kemner, K.M., Bunker, B.A., Fein, J.B., Fowle, D.A., 2003. Adsorption of cadmium to *Bacillus subtilis* bacterial cell walls: a pH-dependent X-ray absorption fine structure spectroscopy study. Geochim. Cosmochim. Acta 67, 3299–3311.
Brassard, P., Kramer, J.R., Collins, P.V., 1990. Binding site analysis using linear programming. Environ. Sci. Technol. 24, 195–200.
Cismasu, A.C., Michel, F.M., Tcaciuc, A.P., Tyliszczak, T., Brown Jr., G.E., 2011. Composition and structural aspects of naturally occurring ferrihydrite. Compt. Rendus Geosci. 343, 210–218.
Comte, S., Guibaud, G., Baudu, M., 2006. Relations between extraction protocols for activated sludge extracellular polymeric substances (EPS) and EPS complexation properties. Part I. Comparison of the efficiency of eight EPS extraction methods. Enzym. Microb. Technol. 38, 237–248.
Cox, J.S., Smith, D.S., Warren, L.A., Ferris, F.G., 1999. Characterizing heterogeneous bacterial surface functional groups using discrete affinity spectra for proton binding. Environ. Sci. Technol. 33, 4514–4521.
Craddock, P.R., Dauphas, N., 2011. Iron and carbon isotope evidence for microbial iron respiration throughout the Archean. Earth Planet. Sci. Lethaia 303, 121–132.
Crowe, S.A., Døssing, L.N., Beukes, N.J., Bau, M., Kruger, S.J., Frei, R., Canfield, D.E., 2013. Atmospheric oxygenation three billion years ago. Nature 501, 535–538.
Czaja, A.D., Johnson, C.M., Beard, B.L., Roden, E.E., Li, W., Moorbath, S., 2013. Biological Fe oxidation controlled deposition of banded iron formation in the ca. 3770 Ma Isua Supracrustal Belt (West Greenland). Earth Planet. Sci. Lethaia 363, 192–203.
Eickhoff, M., Obst, M., Schröder, C., Hitchcock, A.P., Tyliszczak, T., Martinez, R.E., Robbins, L.J., Konhauser, K.O., Kappler, A., 2014. Nickel partitioning in biogenic and abiogenic ferrihydrite: the influence of silica and implications for ancient environments. Geochim. Cosmochim. Acta 140, 65–79.
Fein, J.B., Daughney, C.J., Yee, N., Davis, T.A., 1997. A chemical equilibrium model for metal adsorption onto bacterial surfaces. Geochim. Cosmochim. Acta 61, 3319–3328.
Ferris, F.G., Hallberg, R.O., Lyvén, B., Pedersen, K., 2000. Retention of strontium, cesium, lead and uranium by bacterial iron oxides from a subterranean environment. Appl. Geochem. 15, 1035–1042.
Ferris, F.G., Konhauser, K.O., Lyvén, B., Pedersen, K., 1999. Accumulation of metal by bacteriogenic iron oxides in a subterranean environment. Geomicrobiol J. 16, 181–192.
Franzblau, R.E., Daughney, C.J., Moreau, M., Weisener, C.G., 2014. Selenate adsorption to composites of *Escherichia coli* and iron oxide during the addition, oxidation, and hydrolysis of Fe(II). Chem. Geol. 383, 180–193.
Franzblau, R.E., Daughney, C.J., Swedlund, P.J., Weisener, C.G., Moreau, M., Johannessen, B., Harmer, S.L., 2016. Cu(II) removal by *Anoxybacillus flavithermus*-iron oxide composites during the addition of $Fe(II)_{aq}$. Geochim. Cosmochim. Acta 172, 139–158.

Gauger, T., Byrne, J.M., Konhauser, K.O., Obst, M., Crowe, S., Kappler, A., 2016. Influence of organics and silica on Fe(II) oxidation rates and cell-mineral aggregate formation by the green-sulfur Fe(II)-oxidizing bacterium *Chlorobium ferrooxidans* KoFox - implications for Fe(II) oxidation in ancient oceans. Earth Planet. Sci. Lett. 443, 81–89.

Hallbeck, L., Pedersen, K., 1991. Autotrophic and mixotrophic growth of *Gallionella ferruginea*. J. Gen. Microbiol. 137, 2657–2661.

Hegler, F., Posth, N., Jiang, J., Kappler, A., 2008. Physiology of phototrophic iron (II)-oxidizing bacteria: implications for modern and ancient environments. FEMS Microbiol. Ecol. 66, 250–260.

Hohmann, C., Morin, G., Ona-Nguema, G., Guigner, J.M., Brown Jr., G.E., Kappler, A., 2011. Molecular-level modes of As binding to Fe(III) (oxyhydr)oxides precipitated by the anaerobic nitrate-reducing Fe(II)-oxidizing *Acidovorax* sp. strain BoFeN1. Geochim. Cosmochim. Acta 75, 4699–4712.

Jiang, W., Saxena, A., Song, B., Ward, B.B., Beveridge, T.J., Myneni, S.C., 2004. Elucidation of functional groups on gram-positive and gram-negative bacterial surfaces using infrared spectroscopy. Langmuir 20, 11433–11442.

Jones, C., Nomosatryo, S., Crowe, S.A., Bjerrum, C.J., Canfield, D.E., 2015. Iron oxides, divalent cations, silica, and the early earth phosphorus crisis. Geology 43, 135–138.

Kappler, A., Pasquero, C., Konhauser, K.O., Newman, D.K., 2005. Deposition of banded iron formations by photoautotrophic Fe(II)-oxidizing bacteria. Geology 33, 865–868.

Kennedy, C.B., Martinez, R.E., Scott, S.D., Ferris, F.G., 2003. Surface chemistry and reactivity of bacteriogenic iron oxides from Axial Volcano, Juan de Fuca Ridge, North-East Pacific Ocean. Geobiology 1, 59–69.

Konhauser, K.O., 1997. Bacterial iron biomineralization in nature. FEMS Microbiol. Rev. 20 (x), 315–326.

Konhauser, K.O., 1998. Diversity of bacterial iron mineralization. Earth Sci. Rev. 43 (x), 91–121.

Konhauser, K.O., Hamade, T., Raiswell, R., Morris, R.C., Ferris, F.G., Southam, G., Canfield, D.E., 2002. Could bacteria have formed the Precambrian banded iron formations? Geology 30, 1079–1082.

Konhauser, K.O., Newman, D.K., Kappler, A., 2005. The potential significance of microbial Fe(III)-reduction during Precambrian banded iron formations. Geobiology 3, 167–177.

Li, Y.L., Konhauser, K.O., Cole, D.R., Phelps, T.J., 2011. Mineral ecophysiological evidence for microbial activity in banded iron formation. Geology 39, 707–710.

Liu, Y., Alessi, D.S., Owttrim, G.W., Petrash, D.A., Mloszewska, A.M., Lalonde, S.V., Martinez, R.E., Zhou, Q.X., Konhauser, K.O., 2015. Cell surface reactivity of *Synechococcus* sp. PCC 7002: implications for metal sorption from seawater. Geochim. Cosmochim. Acta 169, 30–44.

Lovley, D.R., 2000. Environmental Microbe-Metal Interactions. ASM Press, Washington D. C 310 pp.

Martell, A.E., Robert M.S., 1999. Critical Stability Constants, vol. Vol. 5. Plenum Press, New York, 1999.

Martinez, R.E., Pedersen, K., Ferris, F.G., 2004. Cadmium complexation by bacteriogenic iron oxides from a subterranean environment. J. Colloid Interface Sci. 275, 82–89.

Martinez, R.E., Ferris, F.G., 2001. Chemical equilibrium modeling techniques for the analysis of high-resolution bacterial metal sorption data. J. Colloid Interface Sci. 243, 73–80.

Martinez, R.E., Ferris, F.G., 2005. Review of the surface chemical heterogeneity of bacteriogenic iron oxides: proton and cadmium sorption. Am. J. Sci. 305, 854–871.

Martinez, R.E., Smith, D.S., Kulczycki, E., Ferris, F.G., 2002. Determination of intrinsic bacterial surface acidity constants using a Donnan shell model and a continuous pK_a distribution method. J. Colloid Interface Sci. 253, 130–139.

Martinez, R.E., Smith, D.S., Pedersen, K., Ferris, F.G., 2003. Surface chemical heterogeneity of bacteriogenic iron oxides from a subterranean environment. Environ. Sci. Technol. 37, 5671–5677.

Menard, H.W., Dietz, R.S., 1951. Origin of abrupt change in slope at continental shelf margin. AAPG Bull. 35, 1994–2016.

Mikutta, R., Baumgärtner, A., Schippers, A., Haumaier, L., Guggenberger, G., 2012. Extracellular polymeric substances from *Bacillus subtilis* associated with minerals modify the extent and rate of heavy metal sorption. Environ. Sci.Technol. 46, 3866–3873.

Mloszewska, A.M., Pecoits, E., Cates, N.L., Mojzsis, S.J., O'Neil, J., Robbins, L.J., Konhauser, K.O., 2012. The composition of Earth's oldest iron formations: the Nuvvuagittuq Supracrustal Belt (Québec, Canada). Earth Planet. Sci. Lett. 317, 331–342.

Moon, E.M., Peacock, C.L., 2013. Modelling Cu(II) adsorption to ferrihydrite and ferrihydrite-bacteria composites: deviation from additive adsorption in the composite sorption system. Geochim. Cosmochim. Acta 104, 148–164.

Omoike, A., Chorover, J., 2004. Spectroscopic study of extracellular polymeric substances from *Bacillus subtilis*: aqueous chemistry and adsorption effects. Biomacromolecules 5, 1219–1230.

Ona-Nguema, G., Morin, G., Juillot, F., Calas, G., Brown Jr., G.E., 2005. EXAFS analysis of arsenite adsorption onto two-line ferrihydrite, hematite, goethite, and lepidocrocite. Environ. Sci. Technol. 39, 9147–9155.

Parikh, S.J., Chorover, J., 2007. Infrared spectroscopy studies of cation effects on lipopolysaccharides in aqueous solution. Colloids Surf., B 55, 241–250.

Pecoits, E., Smith, M., Catling, D., Philippot, P., Kappler, A., Konhauser, K.O., 2015. Atmospheric hydrogen peroxide and Eoarchean iron formations. Geobiology 13, 1–14.

Phoenix, V.R., Martinez, R.E., Konhauser, K.O., Ferris, F.G., 2002. Characterization and implications of the cell surface reactivity of *Calothrix* sp. Strain KC97. Appl. Environ. Microbiol. 68, 4827–4834.

Planavsky, N.J., Asael, D., Hofmann, A., Reinhard, C.T., Lalonde, S.V., Knudsen, A., Wang, X., Ossa, F.O., Pecoits, E., Smith, A.J., 2014. Evidence for oxygenic photosynthesis half a billion years before the Great Oxidation Event. Nat. Geosci. 7, 283–286.

Posth, N.R., Huelin, S., Konhauser, K.O., Kappler, A., 2010. Size, density and composition of cell-mineral aggregates formed during anoxygenic phototrophic Fe(II) oxidation: impact on modern and ancient environments. Geochim. Cosmochim. Acta 74, 3476–3493.

Robbins, L.J., Lalonde, S.V., Saito, M.A., Planavsky, N.J., Mloszewska, A.M., Pecoits, E., Scott, C., Dupont, C.L., Kappler, A., Konhauser, K.O., 2013. Authigenic iron oxide proxies for marine zinc over geological time and implications for eukaryotic metallome evolution. Geobiology 11, 295–306.

Robbins, L.J., Swanner, E.D., Lalonde, S.V., Eickhoff, M., Paranich, M.L., Reinhard, C.T., Peacock, C.L., Kappler, A., Konhauser, K.O., 2015. Limited Zn and Ni mobility during simulated iron formation diagenesis. Chem. Geol. 402, 30–39.

Schaedler, S., Burkhardt, C., Hegler, F., Straub, K.L., Miot, J., Benzerara, K., Kappler, A., 2009. Formation of cell-iron-mineral aggregates by phototrophic and nitrate-reducing anaerobic Fe(II)-oxidizing bacteria. Geomicrobiol J. 26, 93–103.

Schmid, G., Zeitvogel, F., Hao, L., Ingino, P., Adaktylou, I., Eickhoff, M., Obst, M., 2016. Submicron-scale heterogeneities in nickel sorption of various cell-mineral aggregates formed by Fe(II)-oxidizing bacteria. Environ. Sci. Technol. 50, 114–125.

Smith, D.S., Ferris, F.G., 2001. Proton binding by hydrous ferric oxides and aluminum oxide surfaces interpreted using a fully optimized continuous pK_a spectra. Environ. Sci. Technol. 35, 4637–4642.

Smith, D.S., Kramer, J.R., 1999. Multi-site proton interactions with natural organic matter. Environ. Int. 25, 307–314.

Straub, K.L., Rainey, F.A., Widdel, F., 1999. *Rhodovulum iodosum* sp. nov. and *Rhodovulum robiginosum* sp. nov., two new marine phototrophic ferrous-iron-oxidizing purple bacteria. Int. J. Syst. Bacteriol. 49, 729–735.

Swanner, E.D., Mloszewska, A.M., Cirpka, O.A., Schoenberg, R., Konhauser, K.O., Kappler, A., 2015a. Modulation of oxygen production in Archaean oceans by episodes of Fe(II) toxicity. Nat. Geosci. 8, 126–130.

Swanner, E.D., Wu, W., Schoenberg, R., Byrne, J., Michel, M., Pan, Y., Kappler, A., 2015b. Fractionation of Fe isotopes during Fe(II) oxidation by a marine photoferrotroph is controlled by the formation of organic Fe-complexes and colloidal Fe fractions. Geochim. Cosmochim. Acta 165, 44–61.

Tamm, L.K., Tatulian, S.A., 1997. Infrared spectroscopy of proteins and peptides in lipid bilayers. Q. Rev. Biophys. 30, 365–429.

Ueshima, M., Ginn, B.R., Haack, E.A., Szymanowski, J.E.S., Fein, J.B., 2008. Cd adsorption onto *Pseudomonas putida* in the presence and absence of extracellular polymeric substances. Geochim. Cosmochim. Acta 72, 5885–5895.

Widdel, F., Schnell, S., Heising, S., Ehrenreich, A., Assmus, B., Schink, B., 1993. Ferrous iron oxidation by anoxygenic phototrophic bacteria. Nature 362, 834–836.

Wu, W., Swanner, E.D., Hao, L., Zeitvogel, F., Obst, M., Pan, Y., Kappler, A., 2014. Characterization of the physiology and cell–mineral interactions of the marine anoxygenic phototrophic Fe(II) oxidizer *Rhodovulum iodosum* – implications for Precambrian Fe(II) oxidation. FEMS Microbiol. Ecol. 88, 503–515.

Xiong, J., Fischer, W.M., Inoue, K., Nakahara, M., Bauer, C.E., 2000. Molecular evidence for the early evolution of photosynthesis. Science 289, 1724–1730.

Xu, Y., Axe, L., Boonfueng, T., Tyson, T.A., Trivedi, P., Pandya, K., 2007. Ni(II) complexation to amorphous hydrous ferric oxide: an X-ray absorption spectroscopy study. J. Colloid Interface Sci. 314, 10–17.